Proc. of the 9th Intl. Conf. of Asian Society for Precision Engg. and Nanotechnology (ASPEN 2022)
15–18 November 2022, Singapore. Edited by Nai Mui Ling Sharon and A. Senthil Kumar
doi://10.3850/978-981-18-6021-8_OR-12-0067

Study on high performance machining optical surface and its post-treatment strategy by active fluid jet polishing

Zexiao Li, Hao Zhang, Xiaodong Zhang# and Fengzhou Fang

State Key Laboratory of Precision Measuring Technology & Instruments, Laboratory of MicroNano Manufacturing Technology, Tianjin University, Tianjin 300072, China
Corresponding Author / Email: zhangxd@tju.edu.cn, TEL: +81-022-2740-3753, FAX: +81-022-2740-3753

KEYWORDS: Ultra-precision machining, High performance, Tool marks, Active fluid jet polishing

Single point diamond turning (SPDT) shows an advantage of high efficiency in form generation since it can produce optical surfaces with sub-micrometer form accuracy directly. However, the machining tool mark is a significant fact that leads to expected diffraction, which will seriously affect the optical performance. Motivated by this, the relationship between optical performance and tool marks distribution is studied to guide for the high-performance machining and an active fluid jet (AFJ) polishing technology for removing diamond turning marks is introduced and investigated. A simulation model of turning marks removal in the AFJ polishing is developed. A series of spot polishing tests are carried out to study the effect of the AFJ polishing parameters on the material removal rate. A spiral polishing test is conducted and the result shows that a preferred value of material removal which is suitable for eliminating the turning marks without destroying the surface form can be determined by the changes of surface profiles and microtopography. Finally, the practicality of the AFJ polishing method is demonstrated on an aluminum surface. The experimental results and the theoretical analysis prove that AFJ polishing technology can lead to the post-treatment of diamond-turned surfaces in a form-preserving manner.

1. Introduction

Single-point diamond turning (SPDT) is promising because of its efficiently in producing optics with sub-micrometer form accuracy and nanometric roughness [1, 2]. However, the method inherently leaves residual tool marks on the diamond-turned surface, which can induce strong undesirable diffraction and stray light effects [3]. As the application scope of ultra-precision optics diversifies, the demand for improved optical surface quality continues to increase.

In recent years, we have carried out many optical free-form surface machining experiments, and the experimental results further prove the serious impact of tool marks [4, 5]. And with the improvement in nonmetallic cutting technology.

At the same time, because cutting is the main method for processing mold, the tool marks will also indirectly affect the performance of injection molding material or glass molding parts. The understanding of influence of tool marks and find ways to improve the optical performance of the optical system, a series of researches based on optical simulation has been done.

Firstly, the tool mark distribution and optical performances were analyzed to guide the high-performance machining of optical surface. Secondly, a post-treatment process based on AFJ polishing is proposed. The form-preserving capability and effectiveness of the AFJ polishing strategy for removing turning marks are presented.

2. Machining performance analysis on optical surface

2.1 Simulation of tool mark-induced optical performance

In the traditional process of SPDT, the workpiece is fixed on the center of the spindle and the tool servo is synchronized with the position on the x–y plane of the machining coordinate system. The common azimuth sampling or constant arc sampling method is employed to plan the machining tool path.

The tool mark effects on the optical performance were investigated via simulation using near-field diffraction in Fourier optics [6]. When the design model of optical surface is machined by the selected parameters, the final surface is a composition of surface form and tool mark pattern. The scallop height and the tool feed are determined by the feedrate, tool nose radius, and the surface shape according to the geometric relationship. Herein, the spot scale along the scatter direction and energy ratio r_p are used to evaluate the optical performance. The spot scale represents the size of the

reflective or refractive beam from the optical components, and the energy ratio is the ratio of energy in the expected region G to that on the whole image plane. Specifically,

$$r_p = \iint_G uu^* \mathrm{d}x\mathrm{d}y \Big/ \iint uu^* \mathrm{d}x\mathrm{d}y \times 100\% \quad (1)$$

where u and u^* represent the optical amplitude and its conjugate complex, respectively.

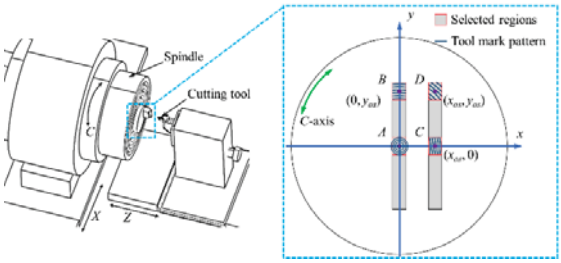

Fig. 1 Schematic of the SPDT and tool mark distribution.

Simulations were conducted on the four regions to investigate the reflective performances of different areas with different tool mark patterns generated by each method, as shown in Fig. 2. The four areas include dense spiral (Region A), quasi-gridline vertical to the scatter direction, namely V-diraction (region B), quasi-gridline along the H-direction (region C), and diagonal quasi-gridline (region D). The simulation of the reflective pattern shows that the high-level diffraction along the H-direction is severe in regions A and B, while loss of energy along the H-direction is avoided in regions C and D.

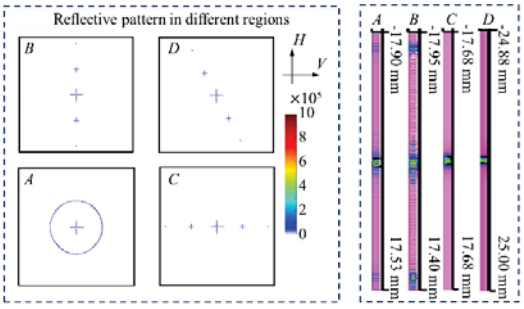

Fig. 2 Simulation results of tool mark-induced optical performance

2.2 SPDT experiment and performance characterization

Machining experiments of large-aspect-ratio optical surfaces were conducted to prove the above simulation. In the experiments, a three-axis ultra-precision machine (Nanotech 250 UPL) was employed to operate the position-optimized off-axis SPDT with a fast tool servo to machine the optical surfaces.

Fig. 3(a) demonstrates the experimental setup and the results of surface quality measured by a Veeco NT9300 white light interferometer. The objective lens was set at 20 with 640×480 pixels. The surface roughness at different areas, including the center and edges, was investigated. The surface roughness is about Ra 5 nm in the optical surface, presenting an optical surface finish.An optical evaluation was conducted to judge the reflective behaviors. Fig. 3(b) demonstrates the experimental setup and the reflective effects, where the light source is 30 mm away from the LRFS. The distance between the workpiece and the screen is 300 mm. The reflective phenomena of Region C and D turning signify the advantages of the proposed machining method. This confirms that the improved tool mark distribution enables high quality optical performance.

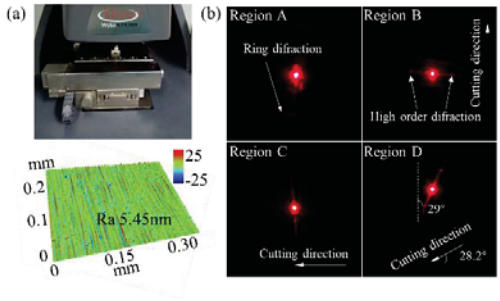

Fig. 3 (a) Surface quality and (b) optical reflective effects.

3. Post-treatment strategy by AFJ polishing

3.1 Principle of AFJ polishing

The AFJ polishing tool is schematically depicted in Fig. 2. This figure shows an aluminum alloy nozzle (yellow part) with an eccentric hole that carries a polishing pin whose diameter is slightly smaller than that of the hole. Typically, the AFJ tool is mounted on the spindle of a CNC machine to generate rotation around the axis of the AFJ tool. During the polishing process, it is moved by the CNC machine to the target location on the workpiece. Meanwhile, a constant flow of polishing slurry is maintained to press the pin (the black part in Fig. 2) against the workpiece. The fluid not only generates the polishing pressure but also streams through the annular gap, thus supporting the polishing area. Similar to most sub-aperture polishing methods, a piece of the polishing pad (such as polyurethane or polishing cloth) is attached to the end surface of the pin which is made of polyethylene or rubber. In addition abrasive particles in the polishing slurry are carried by the polishing pad to remove the SPDT marks.

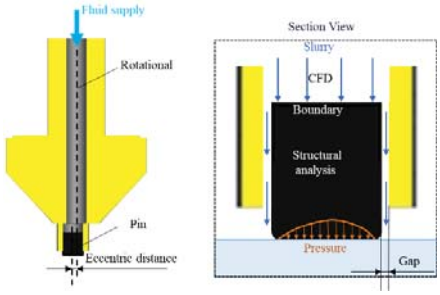

Fig. 3 Schematic diagram of the AFJ polishing tool

The location of the simulated small area P is shown in Fig. 3(a). Here, O_1 and O_2 are the rotational centers of the polishing tool at time T_2 and T_2, respectively. During the process, the polishing tool moves from O_1 to O_2 along a straight line. Moreover, the angle between the instantaneous relative velocity and the turning mark ripples changes from α_{t1} to α_{t2} continuously. The morphology evolution of the surface micro-topography was simulated based on the flowchart proposed above. The simulated results are shown in Fig. 3(b). It is worth noting that the ripple structure is alleviated gradually with an increase in

polishing time, and the periodicity of the turning marks can be eliminated before destroying the substrate. The simulation results indicate that the SPDT marks are removed gradually in the AFJ polishing process, reducing the chances of destroying the substrate. This is an advantage of form-preserved post-treatment strategy for tool mark removal.

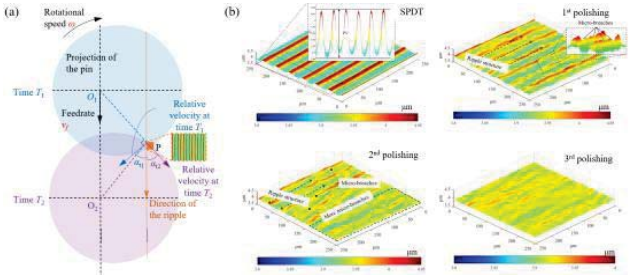

Fig. 4 (a) Motion of the polishing tool and (b) surface microtopography

3.2 Spot polishing test

A series of fixed spot polishing tests were carried out to investigate the TMR in the AFJ polishing process. 18 groups of AFJ polishing experiments with different combinations of process parameters were conducted. For each experiment, the surface texture was measured using a white light Interferometer (Zygo Newview) with a scan size of 0.7 mm × 0.5 mm before and after 2 min of AFJ polishing. Based on the number of process parameters, a 5-factor, 3-level orthogonal table was selected for the polishing experiment. The factors and levels are listed in Table 4. The degree of decline in the PSDTM after AFJ polishing is defined as

$$\Delta PSDTM = PSDTM_{\text{before}} - PSDTM_{\text{after}} \quad (2)$$

where $PSDTM_{\text{before}}$ and $PSDTM_{\text{after}}$ are the logarithms of the PSD value onthe spatial frequency of the turning marks before and after polishing, respectively.

Table 1 Factors and levels of AFJ polishing

Rotation speed (rpm)	Vertical distance (mm)	Eccentric (mm)	Inlet pressure (MPa)	Gap (mm)
100(A1)	1.0(B1)	1.5(C1)	0.05(D1)	0.2(E1)
150(A2)	2.0(B2)	2.0(C2)	0.06(D2)	0.4(E2)
200(A3)	3.0(B3)	2.5(C3)	0.07(D3)	0.6(E3)

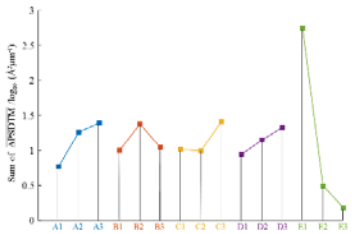

Fig. 5 Influence of process parameters on tool mark removal

The influence of each parameter on the TMR can be assessed by comparing the sum of ΔPSDTM for each level. Fig. 5 illustrates this influence graphically. The combination of A3B2C3D3E1 can yield an efficient TMR. The optimal combination of process parameters are rotation speed of 200 RPM, vertical distance of 2 mm, eccentric distance of 2.5 mm, inlet pressure of 0.07 MPa, and gap a 0.2 mm.

3.3 Spiral polishing test

Spiral polishing tests were carried out to optimize the dwell time in the post-polishing process. The workpiece spindle speed was 7 RPM and the tool feed rate was 0.1 mm/min along X-axis, resulting in an Archimedean spiral path, as shown in Fig. 6. The specimen was initially turned by an SPDT lathe.

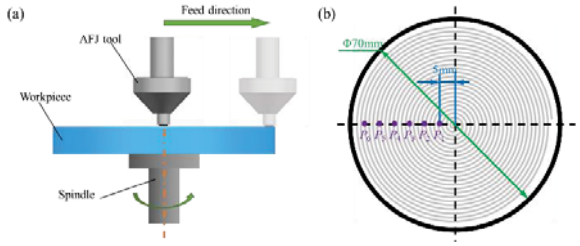

Fig. 6 (a) AFJ tool moving and (b) measurement spots on the surface.

The measuring point after the AFJ polishing is shown in Fig. 6(b). To visually evaluate the form-preserving capability and removal efficiency of the turning marks, the profile of the form change is plotted in the blue line and the PSD amplitudes at all the measurement points are marked in the red squares, as shown in Fig. 7. The PSD analysis was performed based on a line perpendicular to the turning marks. It is worth noting that the roughness (Ra) and PSD amplitude at 1.397 mm^{-1} decrease gradually when the measurement point is close to the center. The turning marks are barely visible at measurement points P1(5 mm), P2(10 mm), and P3(15 mm), and the PSD amplitude is relatively small at these points. From measurement points P4(20 mm) to P6(30 mm), the characteristics of the ripple structure become clear, although there are some microbreaches. both the spindle speed and tool feed rate were held constant in this test; therefore, the velocity increases with increasing distance from the center to the edge. This leads to a gradual decrease in the dwell time of the AFJ tool in each unit area. This means that the SPDT marks were removed gradually with increasing polishing time.

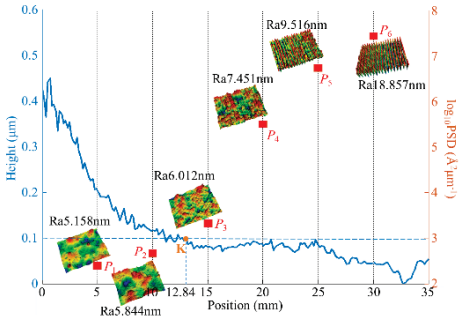

Fig. 7 Influence of process parameters on tool mark removal

Based on the discussion above, a form-preserved post-polishing process can be achieved by adjusting the dwell time and tool path to achieve uniform material removal close to the preferred value, which

is equal to the amount of material removed at K. Hence an optimal feed rate tool path is planned for polishing. As shown in Fig. 20, because the rotation speed of the workpiece is constant, the polar angle is $\rho = a\theta$, where $a = \kappa\rho^{-1}$, κ is an coefficient.

4. Application of AFJ polishing

The practicality of the AFR method and the optimal parameters were demonstrated in the AFJ polishing process, which was performed on a CNC machine provided by OptoTech GmbH. A convex spherical aluminum surface with a radius of 100 mm and diameter of 70 mm was used as the sample, and the experimental setup is shown in Fig. 8. Before polishing, the surface was turned by an SPDT lathe. The optimal feed rate tool path is planned according to Section 3.3.

Fig. 8 AFJ polishing machine tool and polishing path

A comparison of the surface accuracy between the initial and AFJ polished surfaces is shown in Fig. 28. All the results were measured using a laser interferometer (Zygo GPI). The form change map is shown in Fig. 28c. Such small form changes can be neglected.

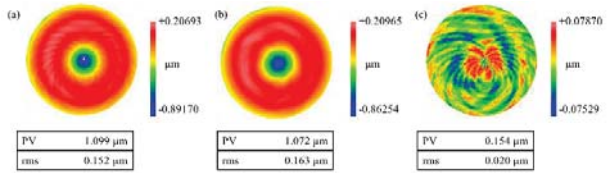

Fig. 9 Surface topography. (a) initial surface; (b) after AFJ polishing; (c) material removal.

The surface roughness was measured using a white light interferometer (Zygo Newview) with a scan size of 0.70 mm × 0.53 mm. Fig. 10(a) is the initial surface roughness. The roughness reduced to 3.309 nm Ra after AFJ polishing, as shown in Fig. 10 (b). To validate the turning mark removal ability, PSD analysis was performed to visualize the spatial frequency, as shown in Fig. 10(c). After AFJ polishing, the peak disappears. The PSD curves reveal that after AF polishing, the surface quality improved dramatically.

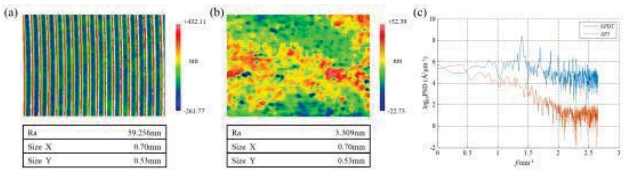

Fig. 10 Surface roughness: (a) initial surface; (b) after AFJ polishing; (c) PSD before and after AFJ polishing.

Pictures of the initial and polished surfaces are shown in Fig. 11. These results show strong evidence of the form-preserving capability and high efficiency of the AFJ polishing method for removing turning marks.

Fig. 11 Surface roughness: (a) initial surface; (b) after AFJ polishing; (c) PSD before and after AFJ polishing.

5. Conclusion

In this paper, influences of the machining properties between the tool mark distribution and optical performances were analyzed to guide the high-performance machining of optical surface. Moreover, an AFJ polishing-based post-treatment strategy is proposed to to remove periodic marks from diamond-turned surfaces is proposed. The material removal and optimization of polishing process were studied theoretically and experimentally to achieve an efficient and form-preserved polishing technology.

ACKNOWLEDGEMENT

This work was supported by the National Key Research and Development Program of China (2017YFA0701200) and National Postdoctoral Program for Innovative Talents of China (BX20190230).

REFERENCES

1. S. Zhang, S. To, S. Wang, Z. Zhu, “A review of surface roughness generation in ultra-precision machining,” Int. J. Mach. Tool. Manuf., Vol. 91, pp. 76-95, 2015.
2. X. Liu, X. Zhang, F. Fang, Z. Zeng, H. Gao, X. Hu, “Influence of machining errors on form errors of microlens arrays in ultra-precision turning,” Int. J. Mach. Tool. Manuf., Vol. 96, pp. 80-93, 2015.
3. Z. Li, F. Fang, X. Zhang, X. Liu, H. Gao, “Highly efficient machining of non-circular freeform optics using fast tool servo assisted ultra-precision turning,” Opt. Express, Vol. 25, No. 21, pp. 25243-25256, 2017.
4. Z. X. Li, X. L. Liu, F. Z. Fang, X. D. Zhang, Z. Zeng, L. L. Zhu, N. Yan, “Integrated manufacture of a freeform of-axis multi-reflective imaging system without optical alignment,” Opt. Express, Vol. 26, No. 6, pp.7625-7637, 2018.
5. F. Z. Fang, K. T. Huang, H. Gong, Z. J. Li, “Study on the optical refection characteristics of surface micro-morphology generated by ultra-precision diamond turning,” Opt. Laser. Eng., Vol. 62, pp. 46-56, 2014.
6. L. M. S. Brea, F. J. T. Milla, T. Morlanes, “Near-Field Diffraction of Chirped Gratings,” Opt. Letters Vol. 41, No. 17, pp. 4091–9094, 2016.